Electronic Supplementary Information

SEM studies of M(100-24) and M(100-48); M(200-24) and M(200-48); M(400-24) and M(400-48); M(1000-24) and M(1000-48)

SEM images in Fig. S1 and S2 showed that samples of MnO_2 obtained by using different amount of cotton (100–1000 mg) under different reaction condition were all in particle-shaped with rough surface. The size of MnO_2 nanoparticles decreased apparently with increasing the amount of cotton. The virtual reasons were still under investigation. In addition, large amount of residual cotton in M(1000-24) and M(1000-48) could be investigated apparently (Fig. S2a and c).

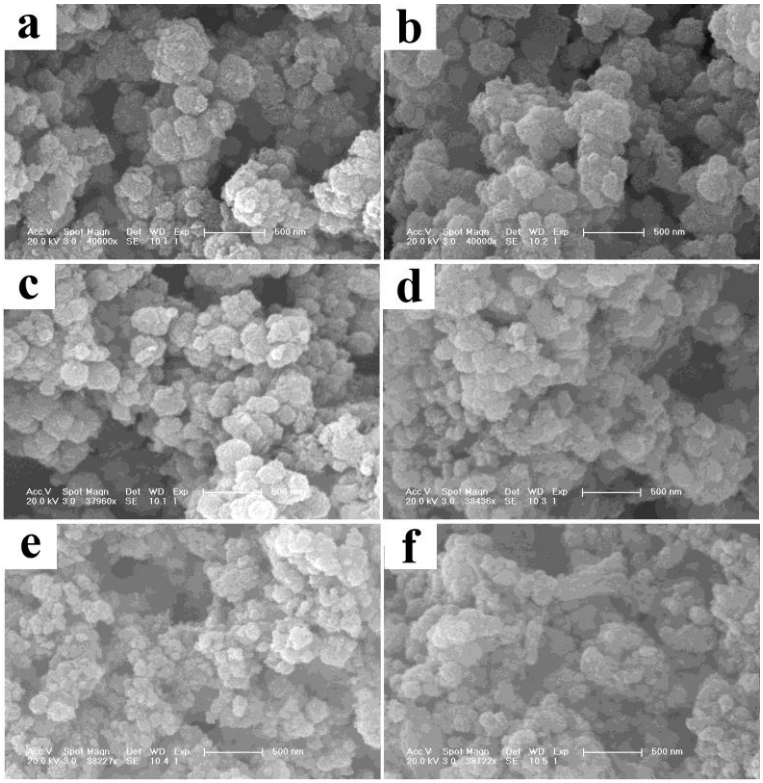

Fig. S1. SEM images of M(100-24) (a) and M(100-48) (b); M(200-24) (c) and M(200-48) (d); M(400-24) (e) and M(400-48) (f).

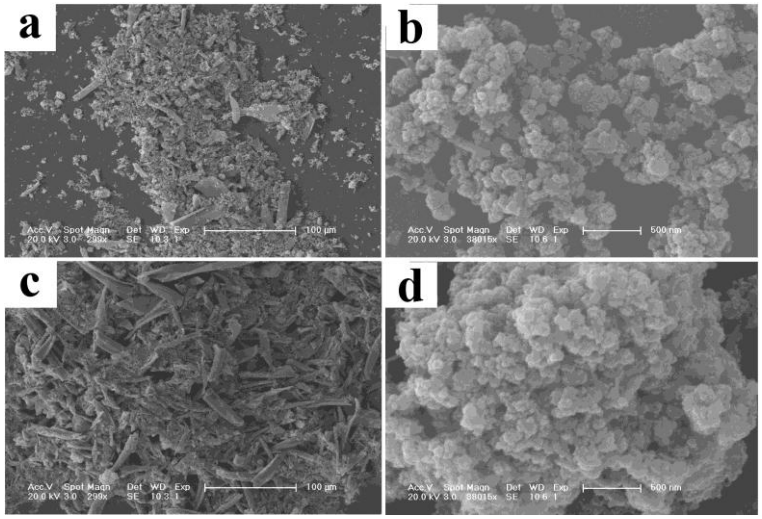

Fig. S2. SEM images with different magnification of M(1000-24) (a, b) and M(1000-48) (c, b).

XRD patterns of M(100-24) and M(100-48); M(200-24) and M(200-48); M(400-24) and M(400-48); M(1000-24) and M(1000-48)

The XRD studies for the prepared MnO_2 at different addition of cotton are shown in Fig. S3. It can be seen from the patterns that the sample prepared by various amount of cotton shows broad peak features which indicate the mixture of amorphous and nanocrystalline nature. This may because that the structures were formed by aggregation of small nanoparticles. There is a decrease in crystallinity with respect to the increase of the amount of cotton as evidenced by the appearance of broader peaks. In XRD patterns of samples when 1000 mg were added, only very weak peaks are observed. The main peaks can be indexed to the α-MnO_2 (JCPDS NO. 44-0141), the broad and low intensity of the signals imply the amorphous nature of MnO_2.[1]

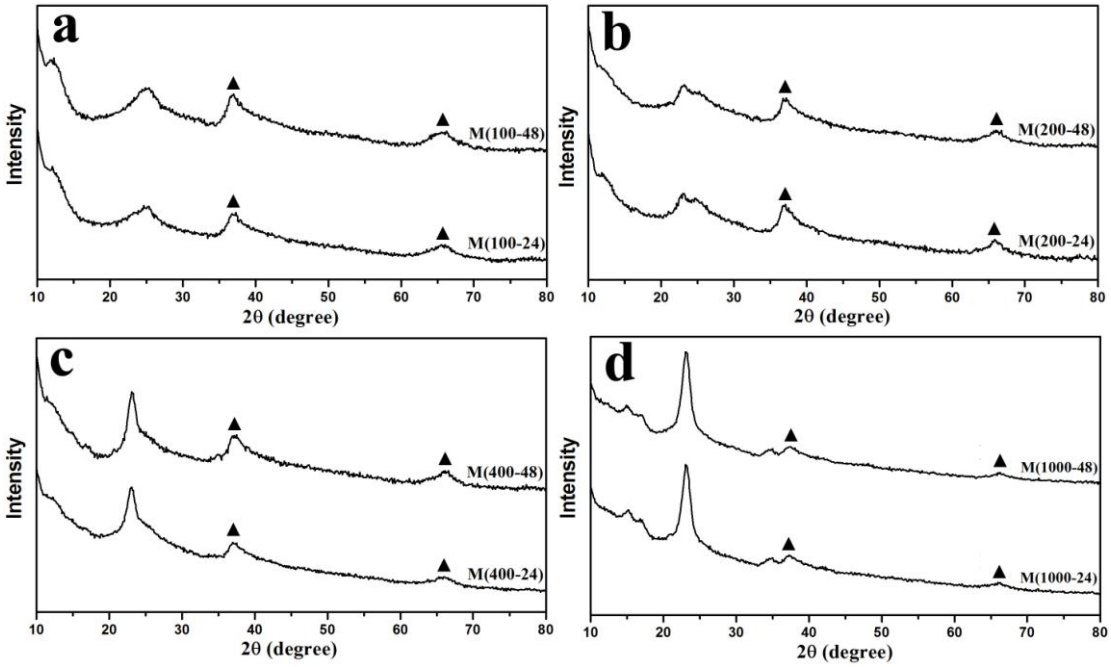

Fig. S3. XRD patterns of M(100-24) and M(100-48) (a); M(200-24) and M(200-48) (b); M(400-24) and M(400-48) (c); M(1000-24) and M(1000-48) (d).

FTIR spectra of M(100-24) and M(100-48); M(200-24) and M(200-48); M(400-24) and M(400-48); M(1000-24) and M(1000-48)

Fig. S4 gives the FTIR spectra of MnO_2 prepared by adding different amount of cotton. The broad band at around 3400 cm^{-1} and the one between 400 and 800 cm^{-1} are attributed to the stretching vibrations of H–O–H and Mn–O bending vibration, respectively.[2] The absorption bands located at about 1420 and 1630 cm^{-1} are assigned to the bending vibrations of OH group of the adsorbed and/or crystalline water molecules.

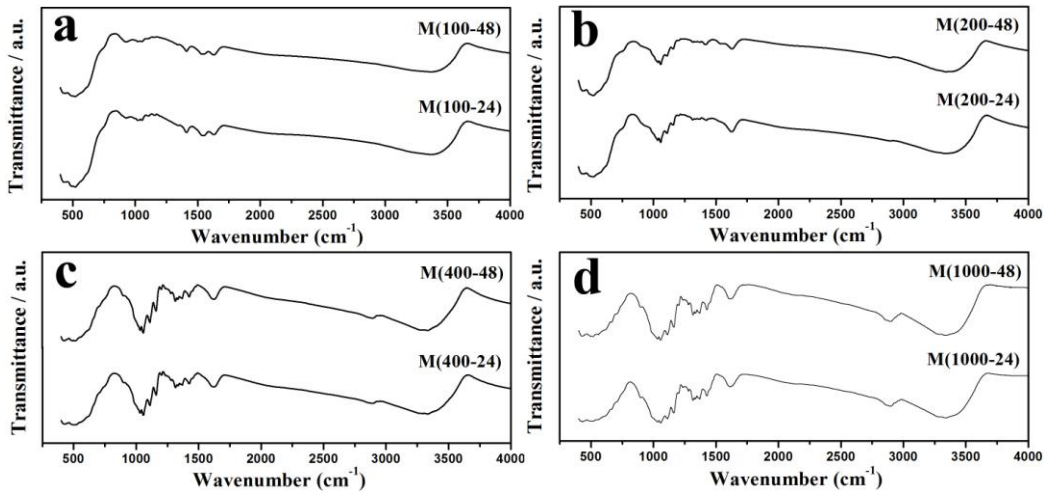

Fig. S4. FTIR spectra of M(100-24) and M(100-48) (a); M(200-24) and M(200-48) (b); M(400-24) and M(400-48) (c); M(1000-24) and M(1000-48) (d).

XPS spectra of M(100-24) and M(100-48); M(200-24) and M(200-48); M(400-24) and M(400-48); M(1000-24) and M(1000-48)

XPS is an effective technique to analyze elements and the corresponding valence state of the material. The Mn 2p and O 1s XPS spectra of other samples are given in Fig. S5–S8. The peak values of other samples also agree well with the reported for MnO_2 and indicate a tetravalence oxidation state for Mn. The O1s spectra can be deconvoluted into three components of Mn–O–Mn bond, Mn–O–H bond and H–O–H bond. In a word, the XPS results are in good agreement with those obtained by other workers in reported literatures.[2]

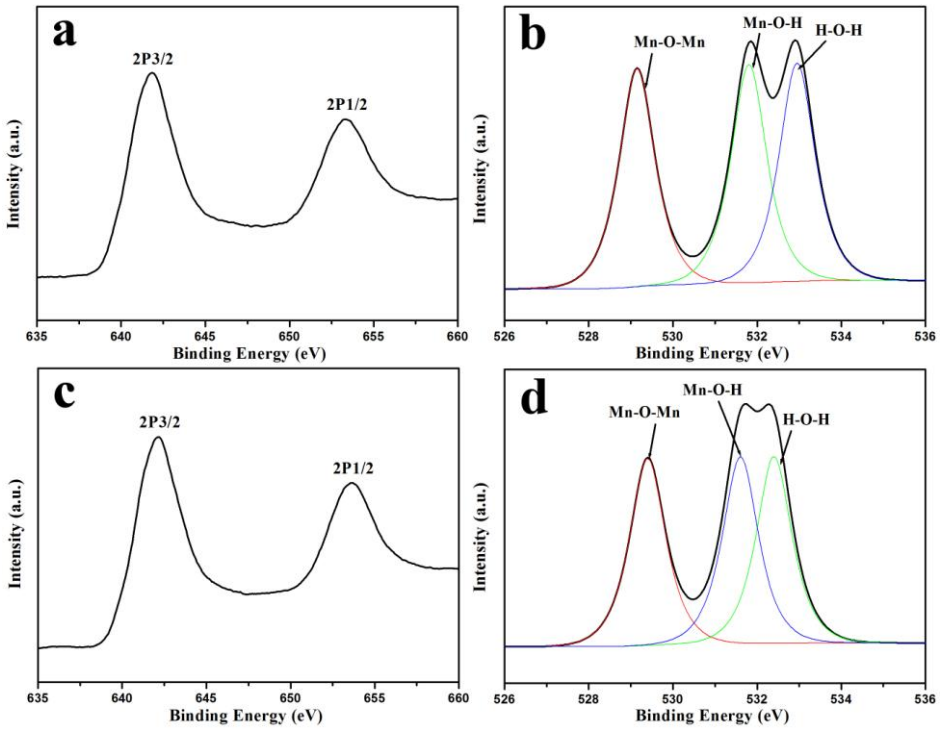

Fig. S5. (a) Mn2p and (b) O1s XPS spectrum of M(100-24); and (c) Mn2p and (d) O1s XPS spectrum of M(100-48).

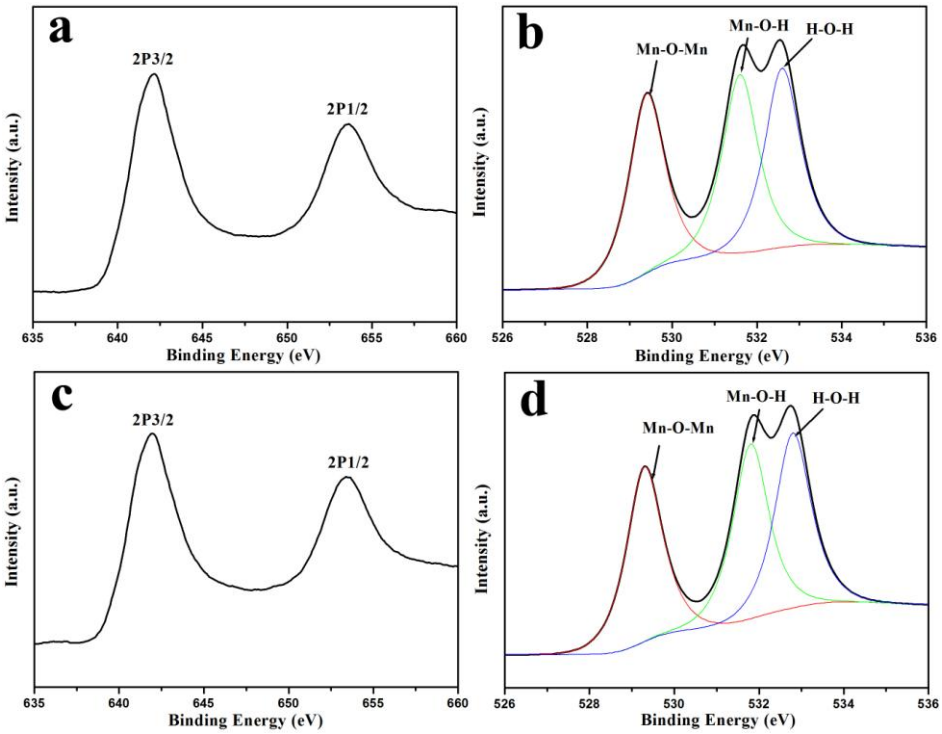

Fig. S6. (a) Mn2p and (b) O1s XPS spectrum of M(200-24); and (c) Mn2p and (d) O1s XPS spectrum of M(200-48).

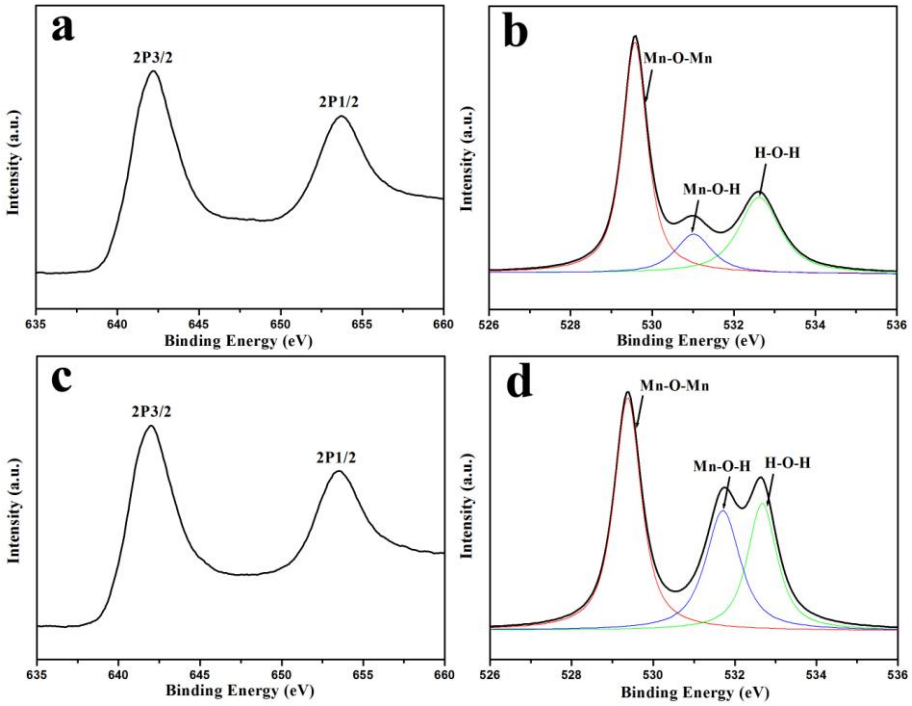

Fig. S7. (a) Mn2p and (b) O1s XPS spectrum of M(400-24); and (c) Mn2p and (d) O1s XPS spectrum of M(400-48).

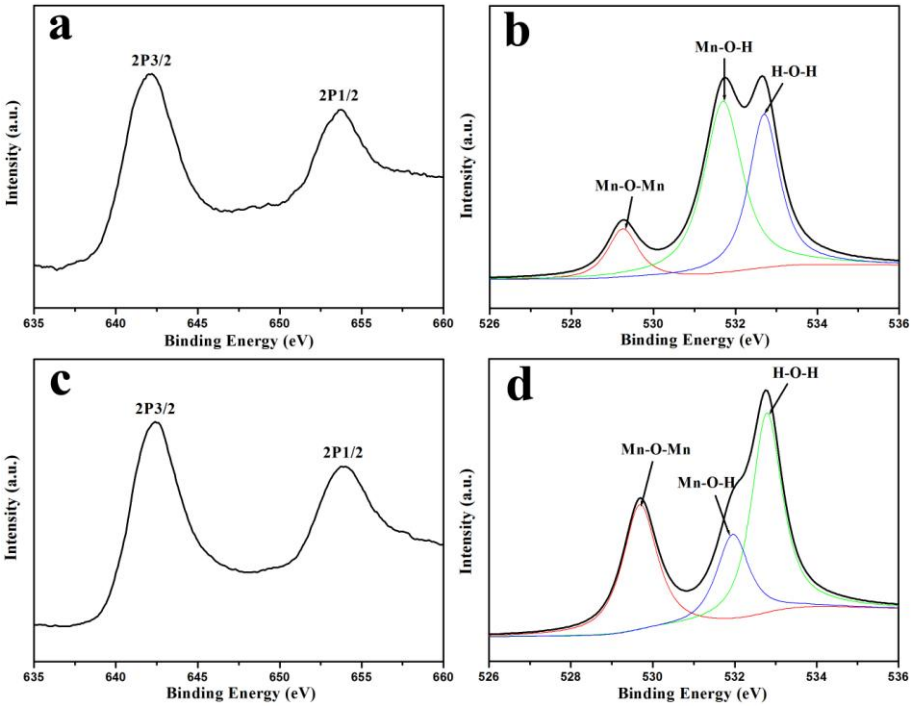

Fig. S8. (a) Mn2p and (b) O1s XPS spectrum of M(1000-24); and (c) Mn2p and (d) O1s XPS spectrum of M(1000-48).

Gas adsorption-desorption isotherm of M(50-12), M(50-24) and M(50-48); M(100-24) and M(100-48); M(200-24) and M(200-48); M(400-24) and M(400-48); M(1000-24) and M(1000-48)

To further investigate the porous structures of the as-prepared products, gas absorption measurement was performed (Fig. S9–S13). From the detailed results of S_{BET}, pore size and pore volume of the samples shown in Table 1 (in main text), the mesoporous nature of them could be well proved.

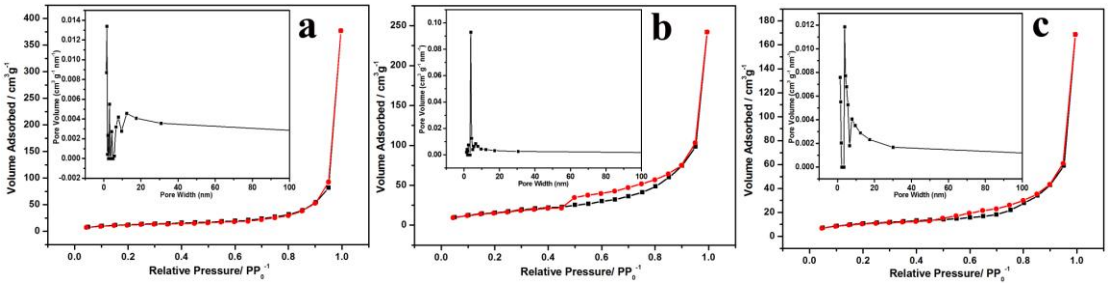

Fig. S9. N_2 adsorption-desorption isotherm of M(50-12) (a), M(50-24) (b) and M(50-48) (c).

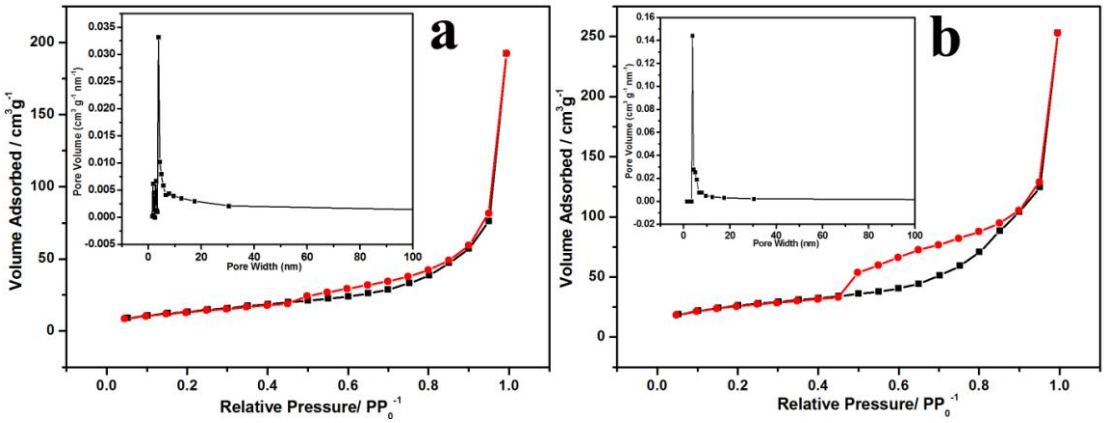

Fig. S10. N_2 adsorption-desorption isotherm of M(100-24) (a) and M(100-48) (b).

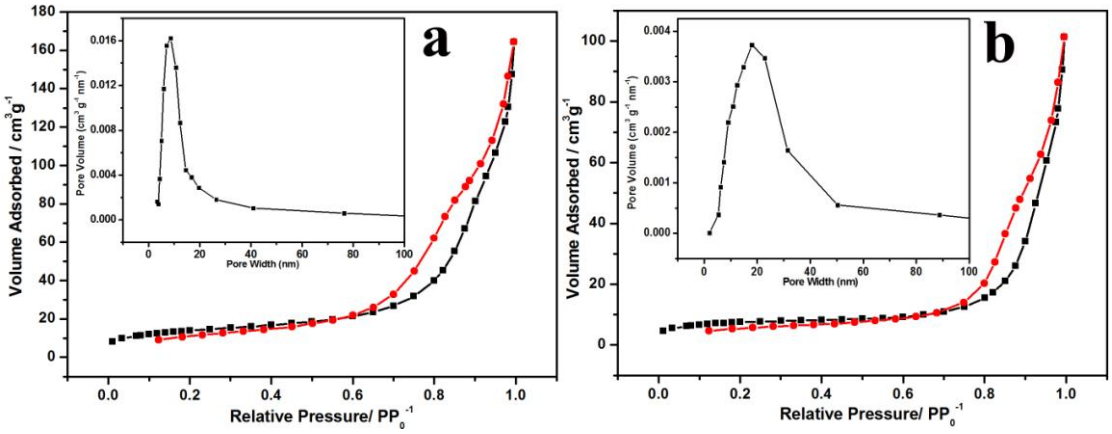

Fig. S11. N_2 adsorption-desorption isotherm of M(200-24) (a) and M(200-48) (b).

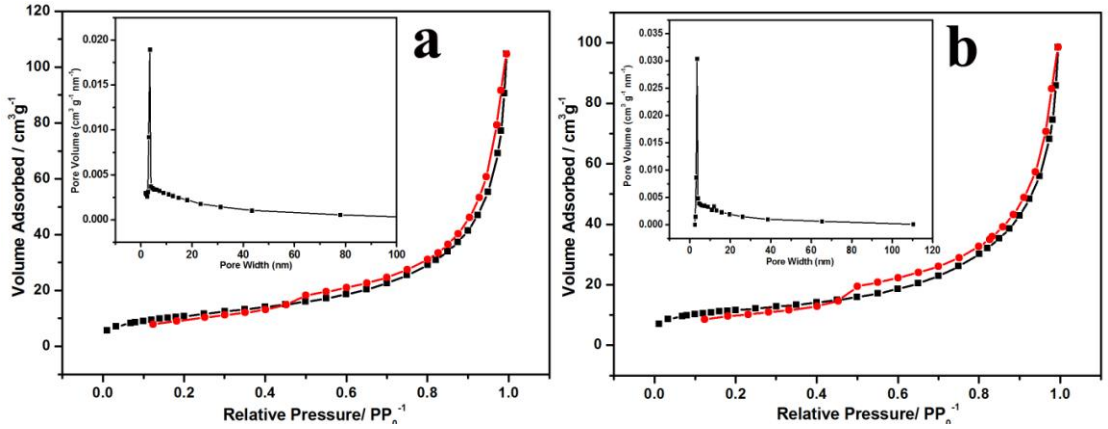

Fig. S12. N_2 adsorption-desorption isotherm of M(400-24) (a) and M(400-48) (b).

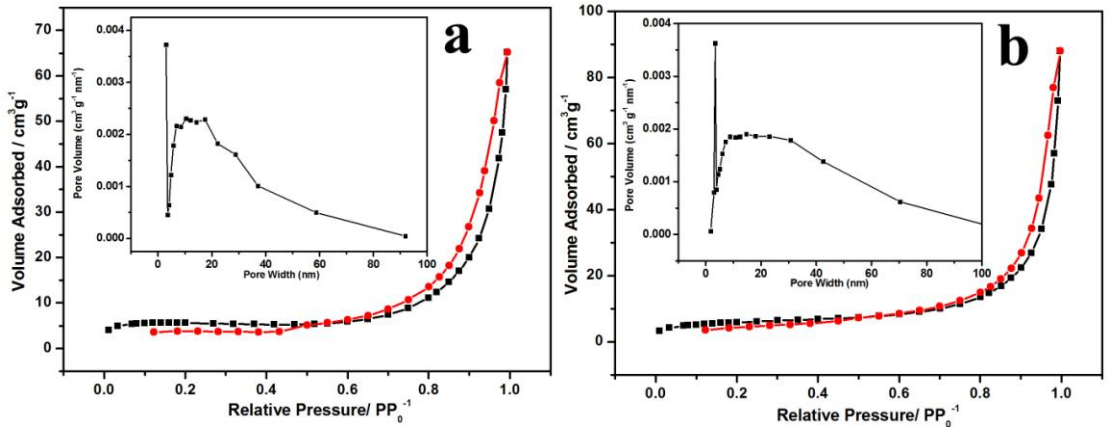

Fig. S13. N_2 adsorption-desorption isotherm of M(1000-24) (a) and M(1000-48) (b).

Cyclic voltammograms of M(100-24) and M(100-48); M(200-24) and M(200-48);

M(400-24) and M(400-48); M(1000-24) and M(1000-48)

Cyclic voltammetry has turned to be an effective experimental technique to evaluate the characteristic capacitive behavior of electrode materials in supercapacitors. Typical CV curves of various amorphous MnO_2 samples shown in Fig. S14–S17 were collected between 0 and 1 V (vs. Ag/AgCl) in 1 mol L^{-1} Na_2SO_4 aqueous solution at varied scan rates (1, 5 and 10 mV s^{-1}) in the three-electrode cell system. Relatively rectangular and nearly mirror-image shaped CV curves demonstrated that the electrode materials possessed high electrochemical reversibility and ideal electrochemical capacitive.[1] The redox peaks in CVs, especially in ones at low scan rates, reveals the pseudocapacitive nature of the present MnO_2. The area surrounded by CV curves shrinks with increasing the scan rate, indicating the decrease of the capacitance value at high scan rate. The SC values of the electrode materials can be calculated from the CV curves using a three-electrode cell system according to the following equation:

$$SC = \frac{Q}{2m\Delta V}$$

where *SC*, *Q*, *m* and ΔV stands for the specific capacitance, voltammetric charge obtained from the integrated area of the CV curves, mass of active electrode material (6 mg) and the sweep potential window. The corresponding SC values were listed in Table S1. It could be found that the SC values decreased with increasing the addition of the mass of cotton.

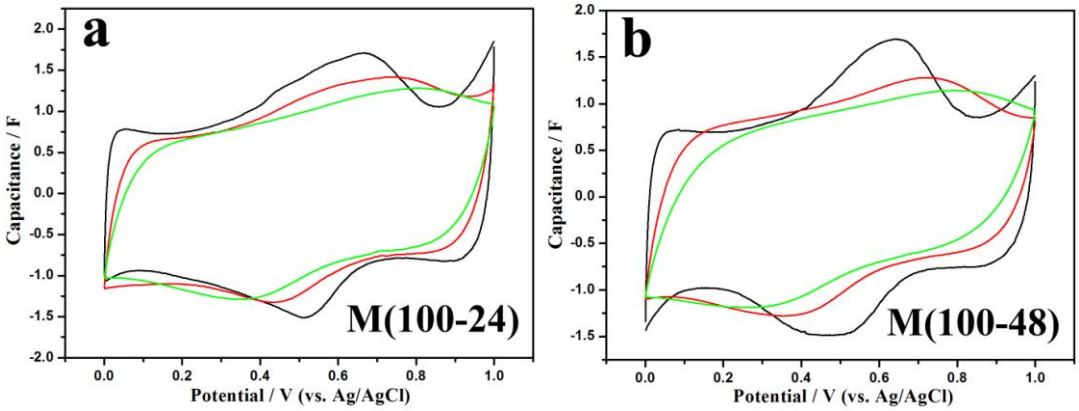

Fig. S14. CV curves of M(100-24) (a) and M(100-48) (b) in 1 mol L^{-1} Na_2SO_4 aqueous solutions at varied scan rates (from inner to outer: 10, 5 and 1 mV s^{-1}).

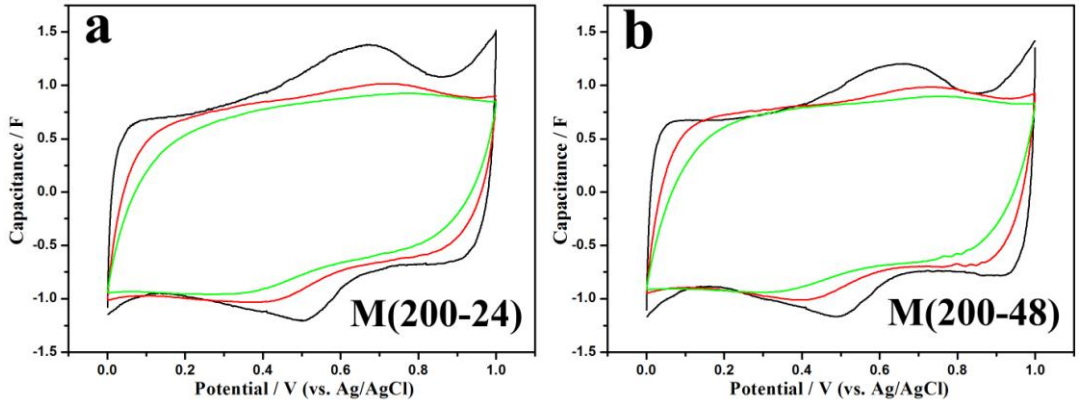

Fig. S15. CV curves of M(200-24) (a) and M(200-48) (b) in 1 mol L^{-1} Na_2SO_4 aqueous solutions at varied scan rates (from inner to outer: 10, 5 and 1 mV s^{-1}).

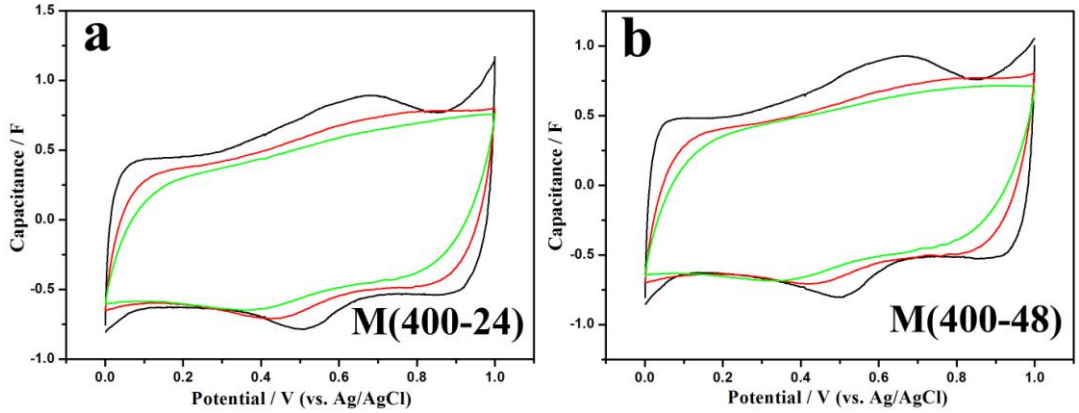

Fig. S16. CV curves of M(400-24) (a) and M(400-48) (b) in 1 mol L^{-1} Na_2SO_4 aqueous solutions at varied scan rates (from inner to outer: 10, 5 and 1 mV s^{-1}).

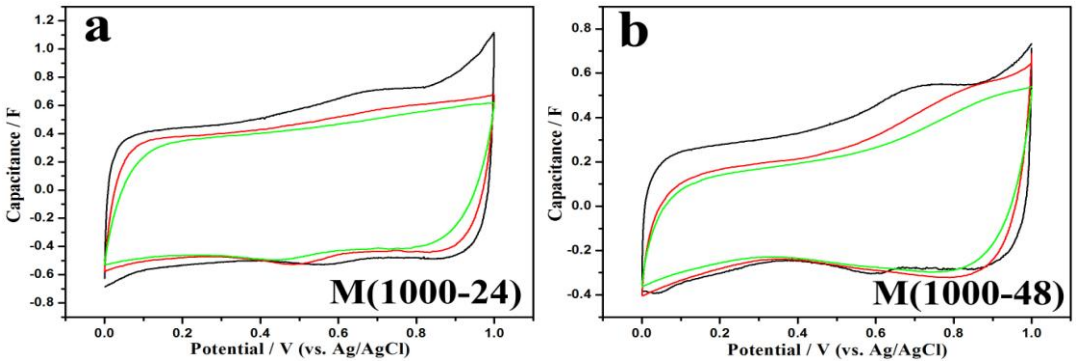

Fig. S17. CV curves of M(1000-24) (a) and M(1000-48) (b) in 1 mol L^{-1} Na_2SO_4 aqueous solutions at varied scan rates (from inner to outer: 10, 5 and 1 mV s^{-1}).

Table S1. Summary for specific capacitance (unit: F g^{-1}) of various MnO_2 electrode materials in 1 mol L^{-1} Na_2SO_4 aqueous electrolytes.

Sample	Scan rate of 1 mV S^{-1}	Scan rate of 5 mV S^{-1}	Scan rate of 10 mV S^{-1}
M(50-12)	178.93	154.52	135.10
M(50-24)	177.40	152.14	133.42
M(50-48)	175.07	152.67	130.25
M(100-24)	179.19	158.99	143.94
M(100-48)	170.62	146.02	126.14
M(200-24)	156.20	128.73	112.04
M(200-48)	148.39	130.36	114.10
M(400-24)	104.76	88.51	76.12
M(400-48)	107.87	89.81	80.27
M(1000-24)	90.04	75.09	67.36
M(1000-48)	56.37	46.35	40.24

References

1 P. Ragupathy, H. N. Vasan and N. Munichandraiah, *J. Electrochem. Soc.*, 2008, **155**, A34.

2 B. Babakhani and D. G. Ivey, *J Power Sources*, 2010, **195**, 2110.